

A quasiclassical approach to electron impact ionization

Tihamér Geyer¹ and Jan M Rost²

¹ Weizmann Institute of Science, Department of Chemical Physics, Rehovot 76100, Israel

² Max-Planck-Institute for the Physics of Complex Systems, Nöthnitzer Strasse 38,
D-01187 Dresden, Germany

Received 5 November 2001, in final form 8 February 2002

Published 13 March 2002

Online at stacks.iop.org/JPhysB/35/1479

Abstract

A quasiclassical approximation to quantum mechanical scattering in the Møller formalism is developed. While keeping the numerical advantage of a standard classical trajectory Monte Carlo calculation, our approach is no longer restricted to using stationary initial distributions. This allows one to improve the results by using better suited initial phase space distributions than the microcanonical one and to gain insight into the collision mechanism by studying the influence of different initial distributions on the cross section. A comprehensive account of results for single, double and triple differential cross sections for atomic hydrogen will be given, in comparison with experiment and other theories.

1. Introduction

Electron impact ionization of hydrogen probes the scattering properties of three charged particles without any influence from passive core electrons or other perturbations. For this reason it has served as a benchmark system for understanding non-separable Coulomb collision dynamics for a long time, which is reflected in the enormous amount of literature and the remarkable theoretical and experimental success in handling these collisions. A milestone was furnished by the experiments by Ehrhardt and his group obtaining fully differential cross sections on an absolute scale [1, 2]. Theoretically, many different approximate treatments have reached increasingly better agreement with experiment [3–7] and fully numerical calculations, first available for the total cross section [8], have reached a breakthrough recently [9] for fully differential cross sections and are now producing results for many impact energies and geometries [10–12].

Our goal with the formulation of a quasiclassical theory of electron impact ionization is to open the way for considering scattering of more than three particles, as already done experimentally with double ionization by electron impact [13, 14]. Furthermore, we aim at a description which allows for a calculation of the entire scattering information (i.e. the whole accessible parameter space in final angles and energies) at once. This is motivated by similar experimental capabilities made possible by the COLTRIMS technique which allows for a new representation of scattering data (see e.g. [15, 16]).

Clearly, with the present computational and theoretical tools this is not possible for four or more particles. One has to fall back on quasiclassical approximations based on the rather successful classical trajectory Monte Carlo (CTMC) method [17]. As will be explained later, there is an obstacle deeply rooted in classical mechanics which has hindered extension of the CTMC method to more than one active target electron. One goal of our work is to overcome this obstacle. In this paper we have restricted consideration to three particles, namely the electron impact ionization of hydrogen, in order to see where the strengths and weaknesses of our quasiclassical approach lie. Also, we would like to make contact with the original CTMC method by deriving it as a limiting case of our approach.

Combining the classical treatment with quantum effects has had a long history in collision theory. Shortly after Abrines and Percival introduced the CTMC method where the target electron was represented by an ensemble of Kepler orbits of fixed energy ('microcanonical distribution'), alternative descriptions were proposed, e.g., the Wigner transform of the quantum wavefunction [18], 'superpositions' of microcanonical distributions of different energies [19, 20] and, only recently, an 'optimum classical description', based on symmetry considerations and phase space partitioning [21]. In an attempt to describe four-body systems, helium was modelled classically in an independent-electron picture or the interaction between the two bound electrons was switched off temporarily to prevent autoionization (see, e.g., [22–24]). All these attempts had in common that they started from the purely classical model and tried to extend it by implementing quantum elements (see, e.g., [25, 26]). Such strategies have limited predictive power, as parameters or switch-on times must be fitted to reproduce particular cross sections.

As briefly reported in [27] we propose an alternative approach: we start from the (exact) time-dependent quantum formulation, translate it to phase space by means of the Wigner formalism and finally approximate this description classically by setting $\hbar = 0$. Hence, we can approximate quantum collisions in a controlled way. Furthermore, we gain additional freedom for the description of the target electron. This leads to an improved agreement of quasiclassical differential cross sections with experiment and, even more important, opens the way to incorporating multi-electron targets without any further approximation to the dynamical description.

The paper is organized as follows: the derivation of the 'quasiclassical' approximation will be given in section 2, in section 3 we will characterize the four initial state distributions that we use for the hydrogen target; the results will be presented and discussed in section 4. The last section contains a conclusion and an outlook to multi-electron targets.

2. The quasiclassical modelling of a collision

We divide the complete ionization process into three parts: setting up the initial state, propagating this initial phase space distribution and finally extracting cross sections from the scattered initial distribution. To arrive at a consistent formulation, each part is treated in the same way by translation into the Wigner picture of quantum mechanics [28]. The classical approximation is subsequently achieved by setting $\hbar = 0$ [29].

2.1. Initial distribution

We construct the initial distribution $w(\vec{p}, \vec{q})$ from the $\hbar = 0$ limit of the Wigner distribution. This distribution is discretized and the individual mesh points in phase space then represent initial conditions for solving classical equations of motion. However, the resulting paths are not those of real electrons in real space; rather they should be interpreted as the evolution

of a discretized phase space density which may have negative parts as well (e.g., for the Wigner distribution). These parts simply contribute to the cross sections with their negative weight; there is no need to argue about ‘negative probabilities’ which clearly demonstrates the advantage of starting with a quantum formulation.

However, naively incorporating such a generalized initial phase space distribution $w(\vec{p}, \vec{q})$ into the usual classical framework leads to other difficulties [18]: in general $w(\vec{p}, \vec{q})$ will not be stationary under the classical propagation, i.e., its Poisson bracket with the Hamiltonian of the unperturbed target does not vanish, $\{H_0^i, w\} \neq 0$. Hence, the initial target distribution will look very different at the time at which the projectile reaches the target and the collision actually happens.

Another problem is even more severe: when using a classical phase space distribution derived from a quantum wavefunction to select initial values for a classical trajectory calculation, most of these initial values do not have the energy of the hydrogen ground state, but they start from a range of energies around the binding energy. Consequently, when extracting cross sections, it is not sufficient any more to just test the final energy of one of the electrons, as the other electron’s final energy cannot be calculated as the difference from the mean total energy. In a total cross section this energy spread might be neglected, but cross sections differential in energy would either be convoluted with the initial energy spread or, if the final energy of the two continuum electrons is added up for a specific trajectory, only trajectories with those initial conditions from the initial distribution which initially started on the energy shell actually contribute. We will explicitly address this problem, which has not been mentioned in previous calculations using non-microcanonical initial distributions [18–20].

Next, we will propose a formulation for the propagation and the extraction of the cross section that can deal with the difficulties arising from general initial distributions.

2.2. Propagation

Quantum mechanical time-dependent scattering is described by calculating the amplitude of transition between the initial and final state through the S -matrix, which is in turn related to the T -matrix describing the cross section directly; see, e.g., [30]:

$$S_{fi} = \langle f | \Omega_-^\dagger \Omega_+ | i \rangle, \quad (1)$$

where

$$\Omega_\mp = \lim_{t \rightarrow \pm\infty} U^\dagger(t) U_0(t) \quad (2)$$

are the Møller operators. The meaning of Ω_+ , e.g., is to propagate backwards with $U_0(t) = \exp[-iH_0^i t]$ using the asymptotic initial Hamiltonian H_0^i without the projectile–target interaction and then forward under the full Hamiltonian with $U(t)$. If the initial and final states are eigenstates of the asymptotic Hamiltonians H_0^i and H_0^f , often a short version is used:

$$S_{fi} = \lim_{t \rightarrow \infty} \langle f | U(t) | i \rangle. \quad (3)$$

By a Wigner transform, the quantum time evolution operator $U(t)$ can be directly transformed with the help of the quantum Liouville operator \mathcal{L}_q , which reduces to the classical Liouville operator \mathcal{L}_c in the limit $\hbar \rightarrow 0$ [31]. The latter describes the evolution of a phase space distribution $w(\vec{p}, \vec{q}, t)$ according to the Poisson bracket

$$\partial_t w = \{H, w\} \equiv -i\mathcal{L}_c w \quad (4)$$

in analogy to the quantum evolution of the density matrix ρ generated by the commutator,

$$\partial_t \rho = -i[H, \rho]. \quad (5)$$

Hence, we could directly use the translation of (3) to classical mechanics via the Liouville operator. In connection with the microcanonical initial state distribution this is indeed equivalent to the CTMC formulation [32, 33].

However, equation (3) is insufficient if the distribution is not stationary under the initial asymptotic propagation. Instead, one must use the complete form (1) of the scattering operator $S = \Omega_-^\dagger \Omega_+$. Correspondingly, the Møller operators are translated into a classical propagation scheme, which ‘transforms’ the initial non-stationary phase space distribution $w_i(\gamma)$, where $\gamma = (\vec{p}_1, \vec{q}_1, \vec{p}_2, \vec{q}_2)$ is a point in the 12-dimensional phase space, into the ‘scattered’ result of the reaction $w_f(\gamma)$ at the same point in time:

$$w_f(t=0) = \lim_{t \rightarrow +\infty} \lim_{t' \rightarrow -\infty} e^{i\mathcal{L}_c^f t} e^{-i\mathcal{L}_c(t-t')} e^{-i\mathcal{L}_c^i t'} w_i \equiv \mathcal{K}w_i(t=0). \quad (6)$$

To perform the actual calculation, the initial distribution is discretized, $w_i(\gamma) = \sum_n w_n \delta^{12}(\gamma - \gamma_n^i)$ with the normalization $\sum w_n = 1$. With (6) we get as the final distribution

$$w_f(\gamma) = \mathcal{K}w_i = \sum_n w_n \delta^{12}(\gamma - \gamma_n^f), \quad (7)$$

where each phase space point γ_n^f emerges from γ_n^i through solving successively Hamilton’s equations, first with H_0^i , then with H and eventually with H_0^f . With this propagation scheme a non-stationary initial distribution will spread when being propagated backwards with the asymptotic \mathcal{L}_c^i . However, it will be refocused under the following forward propagation with \mathcal{L}_c . Hence, when the actual collision happens at $t \approx 0$ the original target distribution is restored, slightly polarized by the approaching projectile.

The propagation now compensates for the non-stationarity of the initial distribution, which means, that *any* arbitrary phase space description can be used for the target, even classically unstable multi-electron targets like helium.

The Møller approach is only valid for potentials that fall off ‘fast enough’ as the distance increases. This condition is fulfilled in the initial channel, as the electron is scattered off the neutral target atom. In the final channel, with both electrons being free, we effectively cut off the long-range Coulomb interaction at some large distance R when we switch from the forward to the backward propagation. The scattering amplitude itself is sensitive to the cut-off, but the cross section approaches a well behaved limit as $R \rightarrow \infty$; see, e.g., [30]. In the light of the much more drastic classic approximation of the propagation we have not considered a more sophisticated treatment of the Coulomb interaction, as proposed, e.g., by Dollard [34].

2.3. Extraction of cross sections

According to (1) the cross section is extracted from the overlap between the scattered initial wavefunction $S|i\rangle$ and the asymptotic final state $|f\rangle$, which is an eigenstate of H_0^f . For ionization we assume that $|f\rangle$ can be approximated by two free electrons. However, before we come to the actual evaluation we have to formulate the cross section such that it can make full use of the non-stationary initial phase space distribution $w_i(\vec{p}_1, \vec{q}_1)$, where ‘1’ refers to the target electron. Without modification, the total energy E of the final state forces, by energy conservation for each classical trajectory, only those parts of the initial phase space distribution which have the same total energy E (see above) to contribute to the cross section. However, this would bring us essentially back to the microcanonical description. In order to make the entire non-stationary initial state distribution ‘visible’ to the collision process, we use the energy transfer $\Delta E_1 = E_1^f - E_1^i$ to the target electron rather than its energy E_1^f itself as a differential measure. Of course, as long as the initial state is on the energy shell with a well

defined energy $E = E_1^i + E_2^i$, the new definition coincides with the usual expression for the cross section:

$$\left. \frac{d^5\sigma}{d\Omega_1 d\Omega_2 dE_1} \right|_E = \left. \frac{d^5\sigma}{d\Omega_1 d\Omega_2 d\Delta E_1} \right|_E, \quad (8)$$

where $d\Omega_i$ are the differentials for the solid angles of the two electrons, respectively.

To extract this cross section we have to evaluate the phase space integral [35, 36]

$$\frac{d^5\sigma}{d\Omega_1 d\Omega_2 d\Delta E_1} = \int d\gamma^i \delta(\Omega_1^f - \Omega_1) \delta(\Omega_2^f - \Omega_2) \delta(\Delta E_1^f - \Delta E_1) w_f, \quad (9)$$

where the integration is over the initial state variables with the ‘scattered’ distribution $w_f(\gamma^f) = \mathcal{K}w_i(\gamma^i)$.

The cross section (9) is a generalization of the one derived, e.g., in [35], where the initial target bound state was assumed to live on a torus, i.e., $w_i(\vec{p}_1, \vec{q}_1) = \delta(\vec{I}(\vec{p}_1, \vec{q}_1) - \vec{I}_0)$ with a well defined multi-dimensional action \vec{I}_0 and the initial project state fixes (\vec{p}_2, \vec{q}_2) , except for the impact parameter area $dx_2 dy_2$. Note that the change of variables from the momenta and positions for the scattered distribution w_f to scattering angles and energy transfer in (9) contains a constraint on how a differential phase space volume centred around its guiding trajectory contributes to the cross section: only those phase space cells whose trajectory has the correct energy transfer *and* positive energy after the change of variables are relevant for ionization. Trajectories with correct energy transfer but final negative energy (i.e., one electron is still bound) do not contribute to the ionization cross section. Consequently, if one is interested in the total ionization cross section only, equation (9) simplifies to

$$\sigma_{tot} = \pi b_{max}^2 \sum_{E_1^f, E_2^f \geq 0} w_n \Theta(\Delta E_1^f - \Delta E_1). \quad (10)$$

Finally, we have to respect the Pauli principle for the two identical electrons. This can be done in the initial or final state. The Wigner transformed (anti-) symmetrized asymptotic state wavefunction has two parts: the ‘classical’ part, independent of \hbar , where the indices of the two electrons are interchanged and an ‘interference term’. In the limit $\hbar \rightarrow 0$ the latter part oscillates infinitely rapidly and its contribution to the cross section (9) vanishes upon integration. In the actual calculation it is easier to perform the remaining classical symmetrization in the final state.

3. Initial target phase space distributions

In the previous section we have made a theoretical effort to formulate an approximate scattering theory which goes beyond the classical approximation still using classical trajectories as in the CTMC method. Our goal was to allow for non-stationary initial target distributions in phase space as they occur if one translates the quantum wavefunction into a phase space distribution. This translation, however, is not unique and depends on the correspondence rule used as shown by Moyal [37]; see also [38–40].

Our main interest in this first application of non-stationary distributions is not to optimize the initial distribution but to learn how the collision dynamics is influenced by different aspects of initial distributions. For this purpose we have chosen four prominent distributions for which we will compare the same collision processes. As well as the well known microcanonical distribution, we have chosen Cohen’s ensemble, which is a superposition of microcanonical distributions [20]. In addition to these more classical distributions we will implement the product distribution, the product of the quantum mechanical density in momentum and coordinate space [40], and the well known Wigner distribution [28].

Table 1. Energy spread for the phase space distributions used in our calculations; see the text.

| Distribution | Microcanonical | Cohen | Product | Wigner |
|----------------------------|----------------|-------|---------|--------|
| $\sqrt{(\Delta E)^2}$ (au) | 0 | 0.24 | 1.22 | 0.88 |

All four distributions have the correct expectation value of the binding energy of $E_b = -0.5$ au. However, they have different energy spreading, defined as

$$(\Delta E)^2 = \frac{\int d^3 p d^3 q w(\vec{p}, \vec{q}) (H(\vec{q}, \vec{p}) - E_b)^2}{\int d^3 p d^3 q w(\vec{p}, \vec{q})}. \quad (11)$$

From table 1 one sees that the Wigner and the product distribution have rather broad energy distribution. This is in general the price one must pay for phase space distributions which resemble closely quantum wavefunctions. For later reference we characterize very briefly each distribution.

3.1. The Wigner distribution

From a wavefunction $\psi(\vec{r})$ one obtains the Wigner distribution by means of the reversible transformation [28]

$$w(\vec{p}, \vec{q}; t) = \frac{1}{(2\pi\hbar)^3} \int d^3 s e^{i\vec{p}\vec{s}/\hbar} \psi^*(\vec{q} + \vec{s}/2, t) \psi(\vec{q} - \vec{s}/2, t). \quad (12)$$

By construction, the Wigner function reproduces the quantum probability densities in coordinate and momentum space:

$$\int d^3 p w(\vec{p}, \vec{q}) = |\psi(\vec{q})|^2 \quad \text{and} \quad \int d^3 q w(\vec{p}, \vec{q}) = |\psi(\vec{p})|^2. \quad (13)$$

Note that the Wigner function depends on the angle between \vec{p} and \vec{q} with negative contributions outside the classically allowed region, thus incorporating quantum correlations into the phase space. We have calculated the Wigner function following Eichenauer *et al* [18].

3.2. The product distribution

As the name indicates, the product distribution is defined as the product of the radial quantum probabilities in coordinate and momentum space [40]; in our case for the hydrogen ground state,

$$w(r, p) = \rho(r)\sigma(p) \quad \text{with} \quad \rho(r) = 4r^2 e^{-2r} \quad \text{and} \quad \sigma(p) = \frac{32p^2}{\pi(1+p^2)^4}, \quad (14)$$

where $r = |\vec{q}|$ and $p = |\vec{p}|$. Clearly, by definition the correct quantum density is obtained in coordinate or momentum space as for the Wigner function (13). However, now the directions of \vec{q} and \vec{p} are independent of each other.

3.3. The microcanonical distribution

The microcanonical distribution is the standard (classical) distribution of the CTMC method based on Bohr's model of the hydrogen atom [17]. The classically accessible area of phase space on the energy shell is sampled with equal probability in angle-action coordinates.

This distribution has the ‘correct’ vanishing spread of the binding energy and the correct quantum density in momentum space. However, the coordinate space density

$$\rho_{micro}(r) = \frac{2r^2}{\pi} \sqrt{\frac{2}{r} - 1}, \quad (15)$$

has a cut-off which is not present in the quantum density (cf (14)). Since the microcanonical distribution is derived from Bohr’s atomic model, there exists, of course, no extension for constructing a corresponding classical distribution for more complex targets, e.g., the helium atom. Finally we note that the Wigner distribution, if forced to be on the energy shell, reduces to the microcanonical distribution for hydrogen.

3.4. Cohen’s distribution

In order to preserve the stationarity of the microcanonical distribution, but still come closer to the quantum densities, Cohen proposed another distribution which we will call Cohen’s distribution in the following [20]: it is obtained by summing microcanonical distributions of different energies such that the mean binding energy is correct and only bound orbits contribute. The resulting (analytical) coordinate density is set to the quantum mechanical one. With these constraints the system of equations is already fully determined and the momentum density obtained is only slightly different from the quantum mechanical one. The energy spread of this distribution is small compared to the Wigner or product distribution.

In the following we will see how these four distributions perform under different collisions. Thereby, we will also gain some insight into which properties of the target system are highlighted by a specific cross section.

4. Results for electron impact ionization of hydrogen at three different impact energies

We will present our results for the three different impact energies of 250, 54.4 and 17.6 eV. The choice of these values is motivated by existing experimental data for comparison. At a given impact energy all cross sections, total, single differential and multiple-differential ones, can be extracted from the same numerical data set; see table 2. The only difference is that higher-differential cross sections require many more trajectories to achieve sufficient statistics since only a few hundred out of several million trajectories typically contribute to a fully differential cross section.

For this reason we have carefully implemented the numerical integration of the trajectories. The equations of motion have been regularized to avoid the attractive Coulomb singularities [41] and a sixth-order symplectic integrator [42] with adaptive step-size control has been used. Hence, we are able to handle electron trajectories which directly hit the nucleus. As a consequence the integration is very stable: at a given total energy, fewer than ten trajectories had to be discarded due to a too-large integration error. This stability is important, since the trajectories discarded should be significantly fewer than those contributing to a fully differential cross section.

4.1. Total ionization cross sections

For the microcanonical distribution, the product distribution and Cohen’s energy distribution, every trajectory j has the same weight $w_j = +1/N_{tot}$ in (10) which reduces as a consequence to

$$\sigma_{tot} = \pi b_{max}^2 N_{ion}/N_{tot}, \quad (16)$$

Table 2. Overview of the numbers of trajectories calculated for the various impact energies and initial distributions: b_{max} denotes the maximum impact parameter used; N_{tot} and N_{ion} give the total numbers of trajectories and those contributing to ionization, respectively (cf section 2.3).

| E_{in} (eV) | Distribution | b_{max} (au) | N_{tot} (Mio.) | N_{ion} |
|---------------|----------------|----------------|------------------|-----------|
| 250 | Microcanonical | 3.5 | 6.1 | 155 484 |
| | Product | 12 | 186 | 395 691 |
| | Wigner | 15 | 104 | 339 242 |
| | Cohen | 7.5 | 17.75 | 83 492 |
| 54.4 | Microcanonical | 6 | 20 | 455 781 |
| | Product | 22 | 80 | 162 752 |
| | Wigner | 22 | 181 | 537 997 |
| | Cohen | 9 | 25.67 | 222 888 |
| 17.6 | Microcanonical | 4.5 | 17.5 | 320 244 |
| | Product | 9 | 16.5 | 79 146 |
| | Wigner | 22 | 50.5 | 47 077 |
| | Cohen | 8 | 14.9 | 80 780 |

Table 3. Total ionization cross section in 10^{-17} cm² at the three main impact energies compared to experimental data given by Shah *et al* [43].

| Distribution | E_{in} (eV) | | |
|----------------|---------------|------|------|
| | 250 | 54.4 | 17.6 |
| Microcanonical | 2.76 | 7.24 | 3.27 |
| Product | 2.71 | 8.69 | 3.55 |
| Wigner | 2.52 | 7.91 | 3.98 |
| Cohen | 2.33 | 6.20 | 3.06 |
| Experiment | 3.43 | 6.19 | 2.1 |

the familiar form of standard CTMC. The result for the three impact energies under consideration is given in table 3.

The total cross section was calculated for the energy range from 15 up to 500 eV impact energy. As one can see from figure 1, the overall trend of the experimental cross section is reproduced. However, the energy at the maximum of the cross section is too low by nearly a factor of two and the high-energy limit of the calculations obeys the classical $1/E$ law [44] instead of the quantum mechanical $\ln(E)/E$ behaviour [45]. The fact that all initial state distributions, from the classical microcanonical one to the quantum Wigner distribution, result in the same total cross section to within some ten per cent shows that the deviation from the exact result is mainly due to the dynamical evolution of the distribution during the collision. The classical evolution cannot account for quantum tunnelling, e.g., which becomes relevant for higher impact energies.

Can one hope under these circumstances to obtain reasonable results for differential cross sections? As has been shown previously [4], disagreement on the absolute values of the cross section does not necessarily imply a similar disagreement on the shape of the differential cross sections.

4.2. Single differential ionization cross section

Generally the single differential cross section evolves from a U-shaped form for high energies (figure 2, left panel, at 250 eV) to a flat curve for low energies (figure 2, right panel,

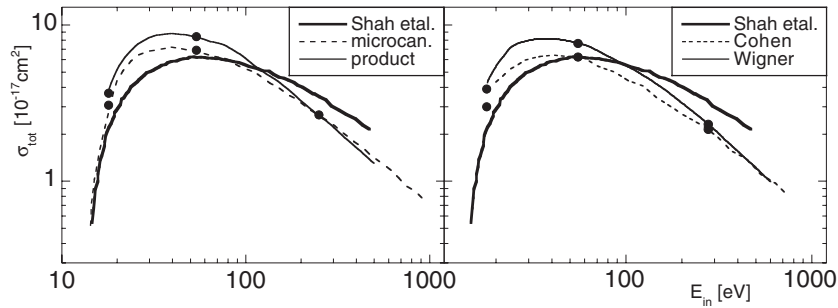


Figure 1. Absolute total ionization cross sections calculated with the four compared initial distributions. The measurements (thick solid curve) are from Shah *et al* [43]. The dots denote the energies at which the differential cross sections were calculated.

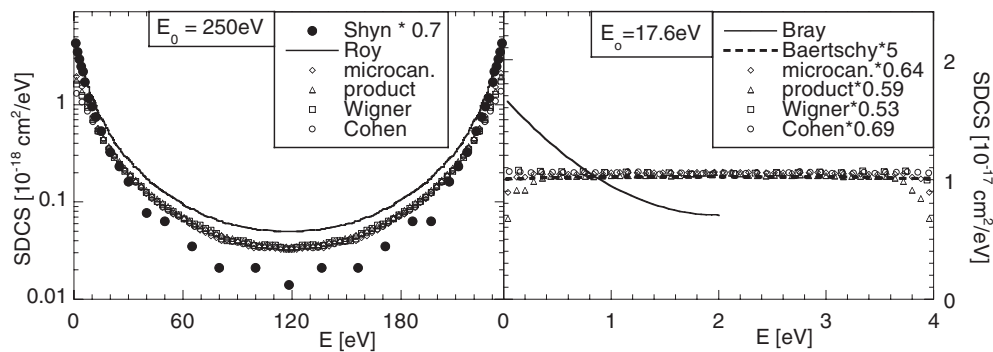


Figure 2. Singly differential cross sections $d\sigma/dE$ for different initial distributions at $E_{in} = 250$ eV (left) and at $E_{in} = 17.6$ eV (right). The measurements by Shyn [46] at 250 eV and our calculations at 17.6 eV are scaled to the correct total cross section. The quantum calculation (solid curve) is from Roy [47]. Comparison at 17.6 eV is made with calculations by Bray [50] and Baertschy *et al* [10]; see the text.

at 17.6 eV). The cross section at 54.4 eV follows this trend and is not shown here. There is little difference between the initial distributions. The agreement with the (scaled) experiment by Shyn [46] as well as with a calculation by Roy [47] employing an exchange-modified Glauber approximation is fairly good at 250 eV. Our result is also consistent with a coupled pseudo-state approximation [48] and a distorted-wave Born calculation [49]. At 17.6 eV the form of the quasiclassical cross section agrees well with results for the $L = 0$ partial wave obtained with two different fully quantal methods, namely exterior complex scaling and a time-dependent CCC method [10]. However, there is clear disagreement with Bray's CCC calculation [50]. In this context it should be noted that towards threshold (13.6 eV impact energy) the contributions of all partial waves should behave as the S-wave contribution [51]. Moreover, the Wannier theory and classical calculations [52] predict a flat cross section to within 5%.

Overall, the single differential cross sections are in good agreement with the experiment and full quantum calculations and they do not provide a critical test for the initial phase space distributions used. However, the very formulation of energy differential cross sections for non-stationary initial distributions has been possible only by the definition of the cross section in terms of the energy transfer (see section 2.3 and table 1).

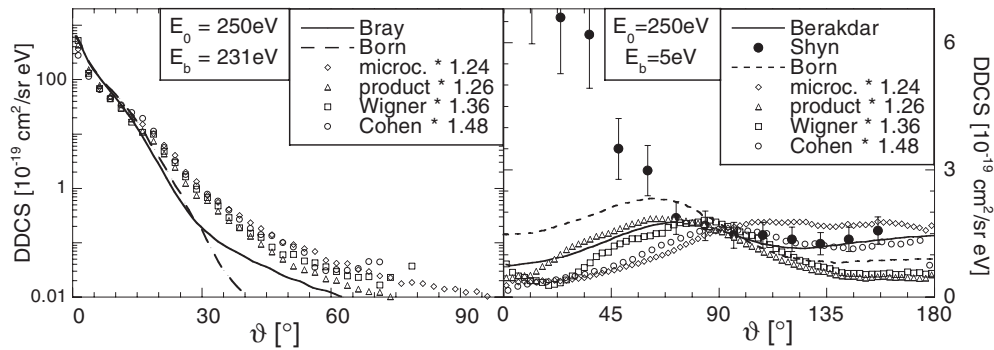


Figure 3. Doubly differential cross sections for the fast ($E_b = 231.4$ eV, left panel) and the slow electrons (5 eV, right panel). The DDCS for the different initial distributions are scaled to give the correct total cross section. The cross sections for the fast electrons are compared to the quantum calculations of Bray [53], those for the slow electrons to the calculation of Berakdar and Klar [6] and the experiments of Shyn [46]. ‘Born’ denotes a first-order Born approximation.

4.3. Multiply differential cross sections at 250 eV impact energy

The impact energy of 250 eV has often been studied, since it is high enough for the first Born approximation to be applicable, but still not too high for a reasonable counting rate in the experiments.

4.3.1. Double differential ionization cross section. As an example for a double differential cross section we present the angular distribution of the electrons for fixed energy sharing of 231.4 + 5 eV. The shape of the different distributions in the left panel of figure 3 for the fast electron is similar and close to that from the quantum calculations (there are no experiments available for this energy).

The situation is quite different for the slow electron (figure 3, right panel). However, the large deviation from the experiment at small angles is probably due to a systematic error in the experiment [46] (see remarks in [6, 53]). More interesting for us is the fact that already, at the level of double differential cross sections, different initial state distributions begin to make a difference. In particular the microcanonical distribution leads to a cross section with an opposite trend compared to the others. The binary peak (around 70°) is almost absent and the cross section is shifted towards larger angles. Apparently, the angular dependence of the scattered slow electron is sensitive to the initial spatial distribution of the bound electron which is not correctly modelled in the microcanonical distribution (see (14), (15)).

4.3.2. Triple differential ionization cross section. For electron impact ionization of hydrogen at an impact energy of 250 eV, a wide range of available data exist, from measured fully differential cross sections (see, e.g., [1, 2, 54, 55]) as well as from calculated ones; for a recent review see [56].

The small volume of the final phase space imposes a serious statistical limit on our quasiclassical calculations: a triply differential cross section at the experimental resolutions of about $\pm 1^\circ$ in the scattering angle of the fast electron and $\pm 2^\circ$ for the slow electron, the definition of the scattering plane at $\pm 10^\circ$ and an energy resolution of less than 1 eV consists of a fraction of less than 10^{-9} of the final state phase space volume only. If the ionization events were equally distributed over the whole phase space, we would hardly find one trajectory for

a cross section. Due to the structure in the pattern of the outgoing electrons, we can record about 100–300 events for those configurations where experimental data are available.

The small number of trajectories contributing to the TDCS forced us to make the bins wider than their mutual distance. With this trick, each event contributes to two or three adjacent data points of the cross section. Still, the comparison with the DDCS shows that the number of propagated trajectories would have to be increased by one or two orders of magnitude for full statistical convergence.

Once the trajectories have been calculated it is easy to filter out cross sections for arbitrary final electron configurations. We will show cross sections for some of the measured data in Ehrhardt geometry, where the fast electron is fixed at a small angle and the angular distribution of the slow electron at a fixed energy is measured: this configuration is very sensitive to the details of the initial distribution and, due to the slow ionized electron, to the dynamics of the reaction. In general two main features appear: the so-called binary peak, located around the direction of the momentum transfer (in the range between 70° and 85°) is usually explained by the classical picture of a binary scattering of the two electrons without interacting with the nucleus. The recoil peak consists of electrons which are rescattered from the nucleus by 180° after the binary encounter. The recoil peak lies roughly opposite to the binary peak (for an overview of the various processes and their explanations, see, e.g., [57]).

Out of the many parameters for which experimental data are available we show two examples from Ehrhardt *et al* [1,2] in figure 4. Angles out of the scattering plane between $\pm 5^\circ$ and $\pm 20^\circ$ have virtually no influence on the shape of the cross section; they only affect the statistics. We set the angular range to $\pm 10^\circ$.

As is clear from figure 4, the microcanonical distribution is not capable of reproducing the main features of the cross section: there is no binary peak (the ‘classical’ part of the cross section) at small momentum transfer and at higher momentum transfer it is much too small and shifted to larger angles. There is some structure in the region of the recoil peak, but as its maximum is opposite to the direction of the fast outgoing electron, this is probably an ‘artifact’ of the calculation.

To describe the recoil peak in a quantum Born approximation, the final state wavefunction for the slow electron has to be a Coulomb wave, i.e., it must include the interaction with the nucleus. The overlap of this infinitely extended wavefunction with the small, localized, radially symmetric ground state selects only the central region of the Coulomb wave, which corresponds to rescattering at vanishing impact parameter. In the classical approximation only a vanishingly small fraction of trajectories lead to a head-on collision with the nucleus after the momentum has been transferred. Hence the probability for rescattering by 180° is negligible and this quantum interpretation of the recoil peak can only be used with caution for the classical approximation. However, one should keep in mind that this picture of the electron recoil from the nucleus comes from the Born perturbation series with its hierarchy of orders, i.e., a number of sudden two-particle interactions take place one after the other [57]. It is only in this interpretation that ionization and rescattering are two distinct events; in the full dynamical description all three bodies interact simultaneously.

The other three distributions perform remarkably better; in particular, with the product and the Wigner distribution the position and the width of the binary maximum are reproduced to within the statistical uncertainties. These two distributions are characterized by the correct densities in coordinate *and* momentum space, whereas Cohen’s energy distribution lacks the correct momentum distribution and the microcanonical one has the wrong spatial dependence. We may conclude that at 250 eV impact energy the cross section is a projection of the initial distribution’s phase space density onto the final configuration: both in momentum and in coordinate space the description of the target must be correct.

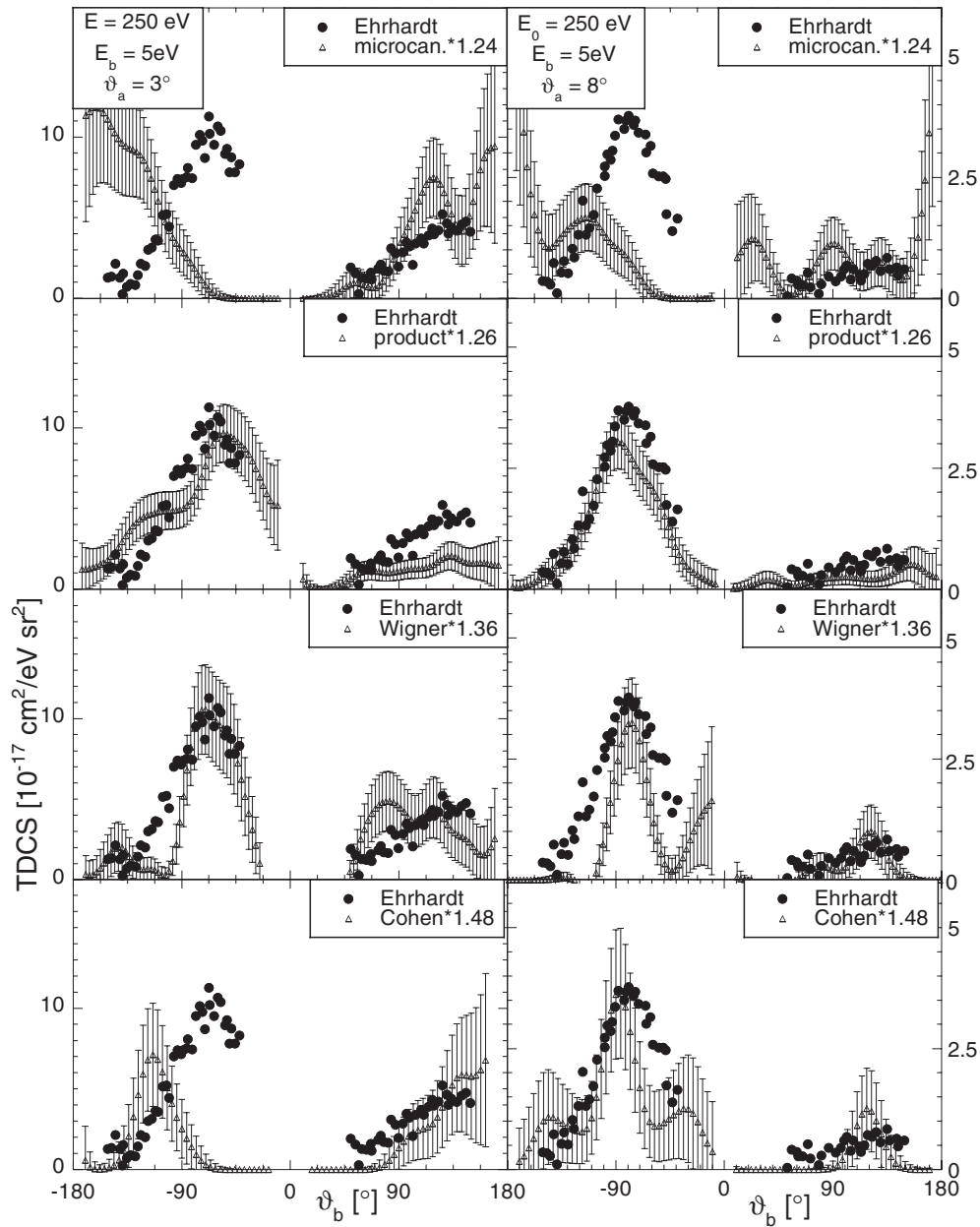


Figure 4. Fully differential cross sections in Ehrhardt geometry. The present calculations are scaled to give the correct total cross section. The absolute measurements are from Ehrhardt *et al* [1].

4.4. Multiply differential cross sections at 54.4 eV impact energy

The impact energy of 54.4 eV is close to the maximum of the experimental total cross section. The presentation of the cross sections will be similar to that at 250 eV.

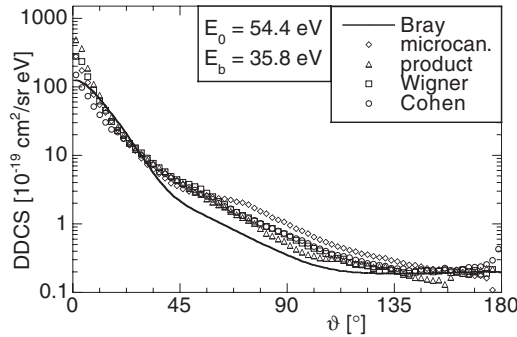


Figure 5. Doubly differential cross sections at $E_{in} = 54.4$ eV of the fast electrons with $E_b = 35.8$ eV: comparison of the quasiclassical results with a CCC calculation by Bray [53].

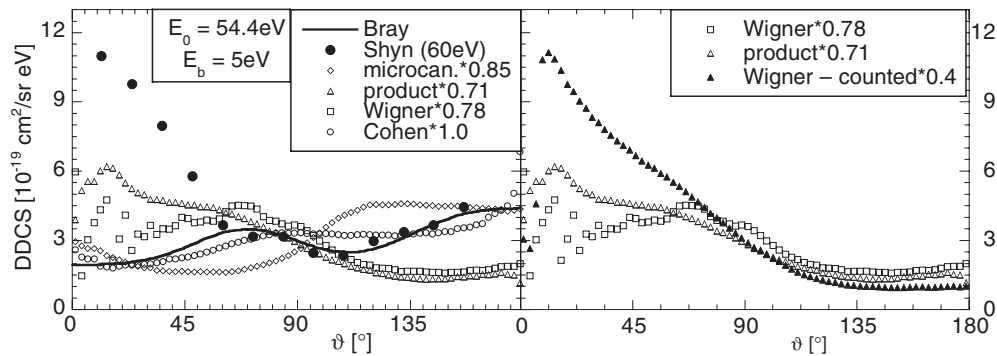


Figure 6. Left: doubly differential cross sections at $E_{in} = 54.4$ eV of the slow electrons with $E_b = 5$ eV. The quasiclassical and the experimental results were scaled to the correct total cross section. The experiment [46] is wrong again at small angles; the full curve is the fully quantum mechanical calculation of [53]. Right: the same as on the left, but here the Wigner result is *not* weighted with the sign of the Wigner distribution; see text for an explanation.

4.4.1. Double differential ionization cross section. The doubly differential cross section is presented again for a pair of matching energies for the fast (figure 5) and the slow electrons (figure 6) with energies of 35.8 and 5 eV, respectively. No experimental data exist for the fast electrons. Comparison is possible, however, with Bray's CCC calculation [53]. For the slow electrons, experiments by Shyn are available, but only at an impact energy of 60 eV. These experimental data were scaled onto the correct total cross section at 54.4 eV. They show systematically too-high values at small angles, similarly to the cases for 250 eV (cf section 4.3.1 and [6, 53]).

The cross sections for the faster electrons are similar (figure 5); the quasiclassical results show slightly higher contributions at angles above 45° , almost independent of the phase space distribution describing the target.

For the slow electrons the picture is quite different (figure 6, left panel): the Wigner distribution reproduces the position of the binary peak (about 70°) and its width fairly well, whereas the microcanonical distribution nearly inverts the shape of the quantum mechanical cross section. Cohen's energy distribution gives a cross section somewhere between the quantum Wigner description and the classical microcanonical modelling.

The cross section from the product distribution is much too high at small angles. This behaviour can be simulated with the Wigner distribution as well, if $|w_n|$ is taken instead of w_n in (10); see the right-hand panel of figure 6.

Table 4. Overview over the parameters for the triply differential cross sections in Ehrhardt geometry extracted at $E_{in} = 54.4$ eV. The angle between the scattering planes was confined to $\pm 12^\circ$.

| E_b (eV) | θ_a | Measured by |
|-------------|---|-------------------------|
| 5 ± 0.5 | $4^\circ \pm 1^\circ, 23^\circ \pm 2^\circ$ | Röder <i>et al</i> [58] |

The Wigner and the product distribution both reproduce the correct density in coordinate and momentum space; the difference is that in the quantum Wigner distribution the radius and the momentum vector are correlated with negative weights in regions outside of the classical turning point (see section 3.1). The difference between the Wigner cross section with the correct sign for each final value and the one with the same sign for each trajectory shows that the contributions at small scattering angles come from these outer regions. The negative parts of the Wigner distribution lead to partial cancellation of classically allowed contributions, which nevertheless do not occur in the cross section. The product distribution lacks the correlations and consequently gives the wrong cross section at small angles; here all trajectories contribute. In the microcanonical distribution no initial values at all exist for radii larger than 2 au; consequently the cross section is much too small for small angles. We conclude that this type of doubly differential cross section strongly depends on quantal features which are beyond the scope of a purely classical ansatz such as the standard CTMC one. However, they can be incorporated in our $\hbar = 0$ approximation through the initial distribution.

4.4.2. Triple differential ionization cross section. The triply differential cross section at 54.4 eV impact energy has been measured by Röder *et al* [58] in Ehrhardt geometry. In figure 7 we show the cross sections for the parameters given in table 4.

The DDCS for the fast electrons, figure 5, is too high for small angles. We therefore not only scale the TDCS onto the total cross section, but additionally for $\theta_a = 4^\circ$ by a factor of 0.25. This scaling has been performed in order to see whether the shape of the cross sections for the slow electrons is reproduced correctly.

The differences between the phase space distributions can be seen clearly: the classical microcanonical distribution fails to reproduce the binary peak at all parameters, whereas the recoil peak agrees astonishingly well. The next more quantal description, Cohen's energy distribution, performs better with increasing θ_a , but the angle of the binary peak is always too large. The opposite tendency, placing the binary peak at too-small angles, is seen with the product distribution. At small θ_a the electrons even leave in the same direction, a configuration that should be strongly suppressed by their mutual repulsion. This problem will be discussed in detail for the impact energy of 17.6 eV. The distribution which is closest to quantum mechanics, the Wigner distribution, can reproduce the cross sections over the entire range of parameters, but with similar effects of both electrons leaving in the forward direction at $\theta_a = 4^\circ$.

At this impact energy, switching from the classical models of the microcanonical or Cohen's energy distribution, which only reproduce either the coordinate or the momentum space density, to the more quantal ones results in a definite improvement in the cross sections. The product distribution, which satisfies both momentum and coordinate space densities, already shows a binary peak, although shifted. With the correlated Wigner distribution the best correspondence between experiment and our calculations is achieved.

4.5. Multiply differential cross sections at 17.6 eV impact energy

At the low impact energy of 17.6 eV the projectile is only moving slightly faster than a classical electron on a circular orbit with the Bohr radius and the ionized electrons can only share 4 eV

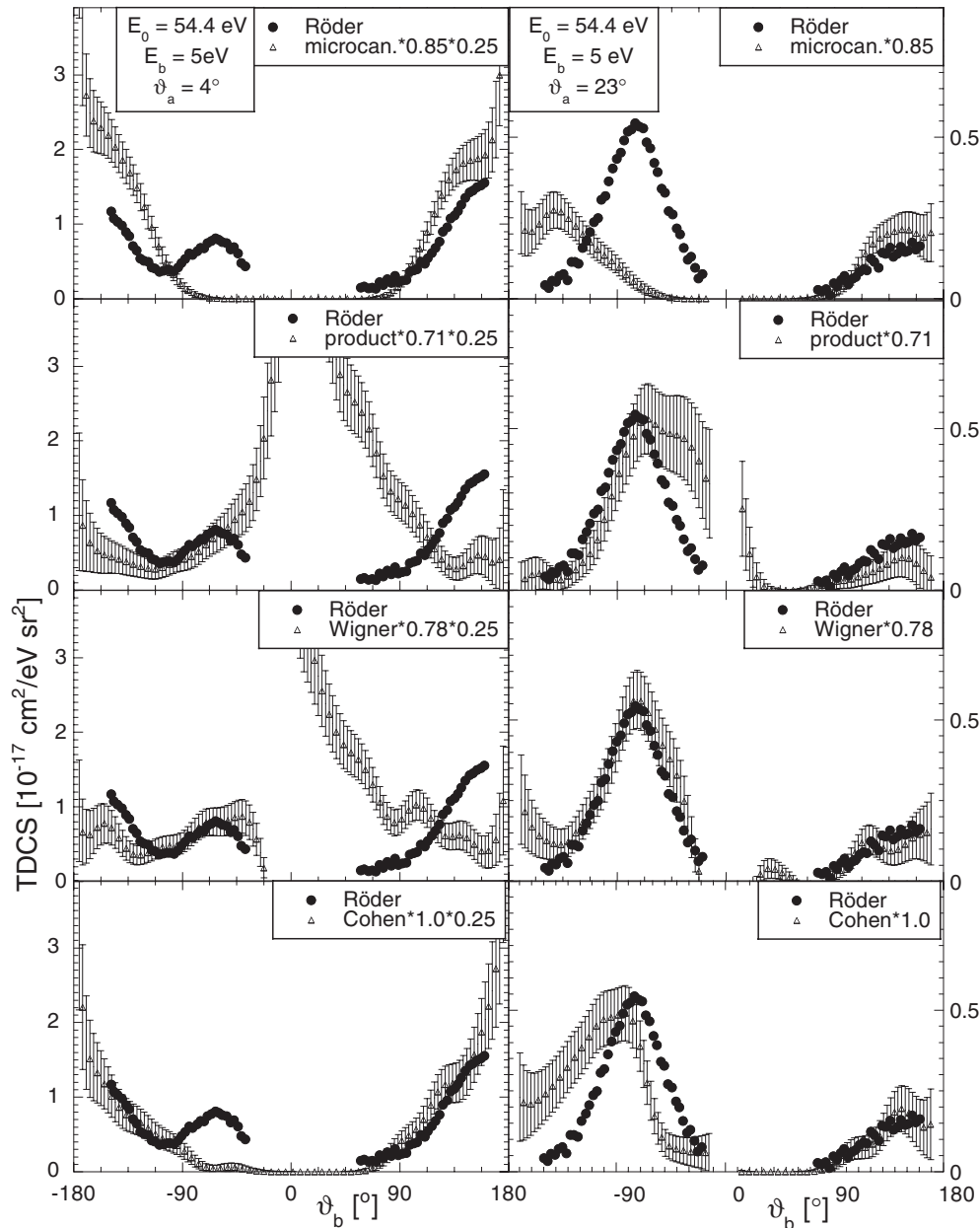


Figure 7. Fully differential cross sections in Ehrhardt geometry at 54.4 eV impact energy for a fixed angle of $\theta_a = 4^\circ$ (left) and 23° (right). The calculations are scaled according to the total cross section and the form of the DDCS (for 4° ; see the text). The absolute measurements are by Röder *et al* [58].

of energy. Hence, we expect different qualities of the initial distribution to become important, compared to the case for higher impact energies.

At these low energies quantum calculations, using analytic final state wavefunctions constructed from two-body wavefunctions, fail or perform only very poorly [56]. This indicates that here a correct description of the simultaneous interaction of the three particles is crucial.

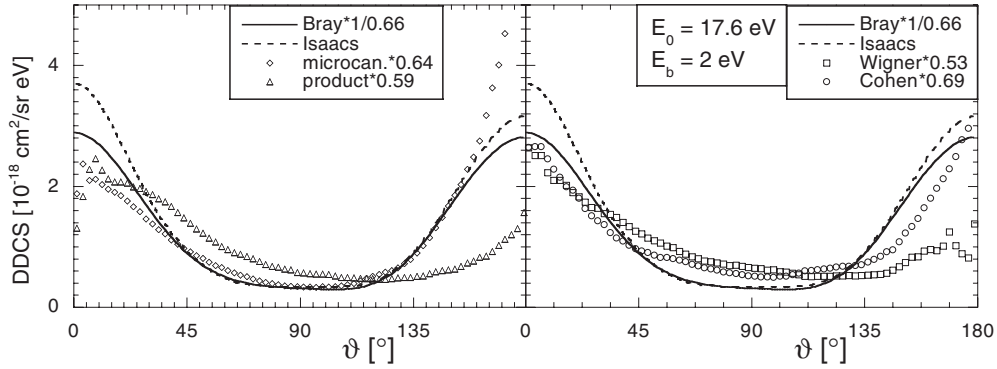


Figure 8. Angular distributions of the electrons with $E_b = 2$ eV at $E_{in} = 17.6$ eV, scaled onto the total cross section, compared to quantum calculations by Bray [50] and Isaacs *et al* [12]. For the scaling, see the text and figure 2.

Table 5. Overview over the geometries and parameters shown for the TDCS at $E_{in} = 17.6$ eV. For all cross sections the scattering plane is confined to $\pm 12^\circ$. The measurements were done by Röder *et al* [58, 59].

| Geometry | Extraction parameters |
|------------------------|---|
| Symmetric | $ \theta_a + \theta_b \leq 8^\circ, E_a - E_b \leq 0.3$ eV |
| Asymmetric | $\theta_a = 60^\circ \pm 3^\circ, E_b = 2 \pm 0.2$ eV |
| Constant θ_{ab} | $\theta_{ab} = 90^\circ, 180^\circ \pm 5^\circ, E_b = 2 \pm 0.2$ eV |

In this context it should be emphasized that we do not approximate the three-body dynamics beyond the classical $\hbar = 0$ limit: all long-range Coulomb interactions between all particles are taken fully into account.

4.5.1. Double differential ionization cross section. For the DDCS no experimental comparison exists; our results will be compared to Bray's CCC calculation [50] and to results of an ECS calculation by Isaacs *et al* [12]. For symmetric energy sharing, the CCC single differential cross section is too small by approximately one third; hence the CCC DDCS was scaled by $1/0.66$ for better comparison of the shape. Our results are scaled onto the total cross section again.

As can be seen in figure 8, the more classical phase space distributions give considerably better results. With the microcanonical distribution the cross section deviates only for angles of less than 30° around the forward and backward direction. With Cohen's distribution the shape is too flat, whereas the Wigner and the product distribution overestimate the forward direction. Both electrons have the same small final energy, which means that they influence each other for a long time. Consequently, these cross sections are more dominated by the post-collisional interaction (PCI) than those at higher energies. In order to describe PCI effects correctly, the relative energy of the outgoing electrons is important. Due to our construction of the cross section in terms of the energy transfer, this ratio is correctly described only for initial distributions on the energy shell (i.e. without an energy spread).

4.5.2. Triple differential ionization cross section. At this impact energy experiments exist for a variety of geometries [58, 59]. Table 5 summarizes them for the cross sections shown. For an overview of recent quantum calculations see [11, 50].

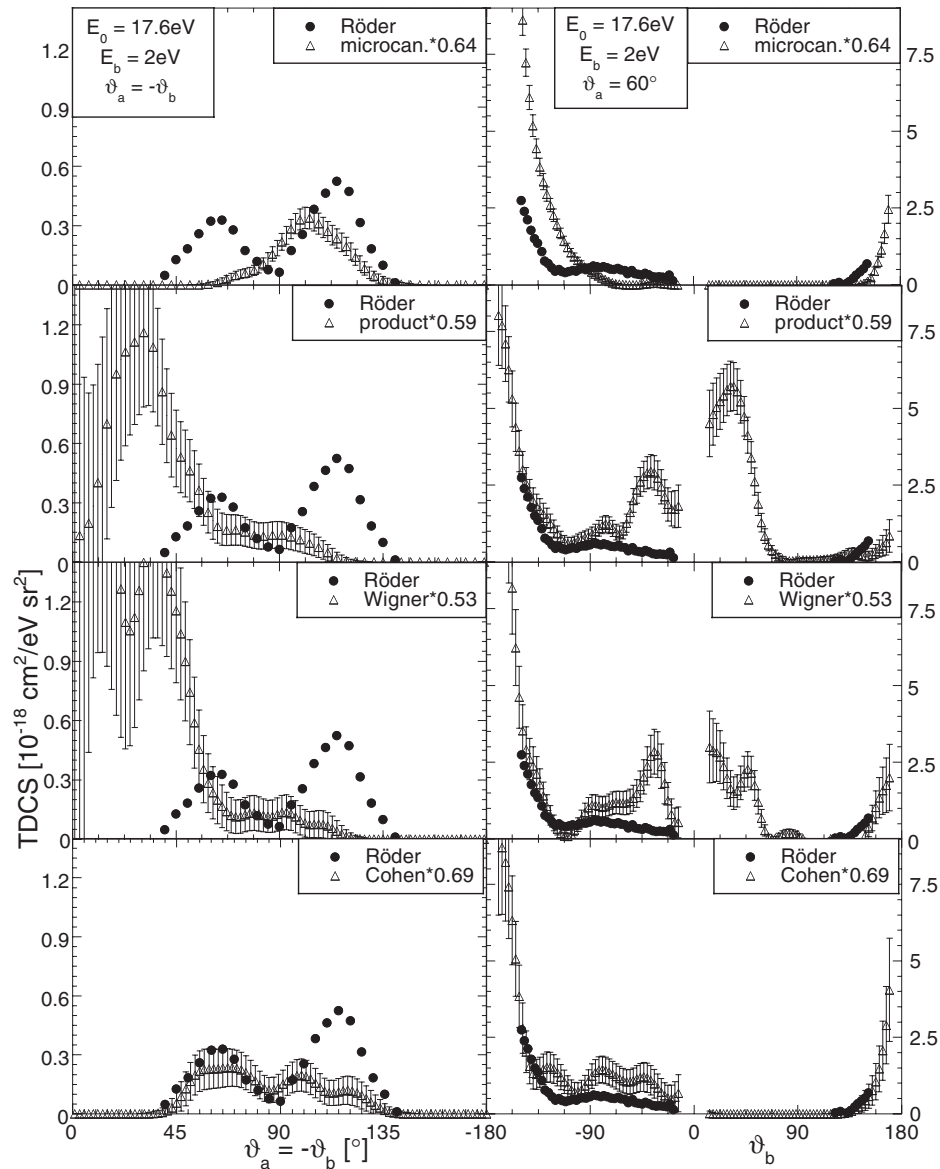


Figure 9. TDCS for a total energy of 4 eV: fully symmetric, i.e. $\theta_a = -\theta_b$ and $E_a = E_b = 2 \text{ eV}$, on the left side and on the right side in Ehrhardt geometry for $E_b = 2 \text{ eV}$ and $\theta_a = 60^\circ$ for the four initial distributions. The cross sections are scaled onto the total cross section.

For the Wigner and the product distribution the same behaviour as at $E_{in} = 54.4 \text{ eV}$ can be observed, but now the fraction of electrons going in the same direction is much larger; see the fully symmetric cross section and, in Ehrhardt geometry, figure 9. This should not occur due to the mutual repulsion of the electrons. However, for those initial distributions which are not restricted to the energy shell (all but the microcanonical one), the energy of the initially bound electron calculated from the energy transfer does not necessarily correspond to the actual momentum of the electron. Hence, the two electrons may leave the nucleus one

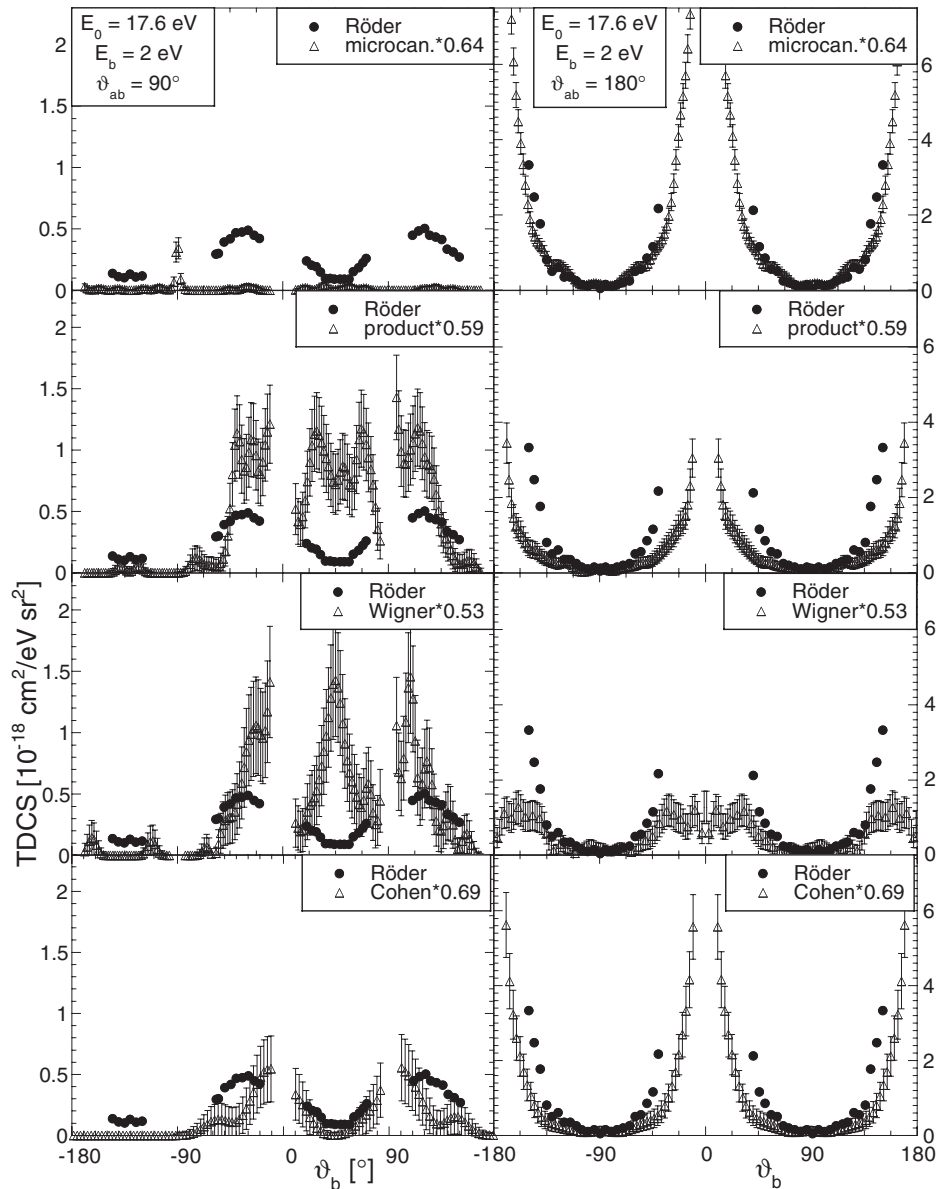


Figure 10. TDCS for constant angle between the electrons: left: with $\theta_{ab} = 90^\circ$; right: at 180° . The cross sections are scaled onto the total cross section.

after the other, although they have the same ‘nominal’ energy. This problem does not occur for the microcanonical distribution which is on the energy shell.

At 17.6 eV impact energy, none of the initial distributions can fully reproduce the cross sections, but in the overall picture Cohen’s distribution works best: on the one hand, the energy spread is small enough to prevent the electrons from going in the same direction and, on the other hand, the phase space density is still accurate enough for the ‘fast’ binary ionization process. Hence, Cohen’s distribution is the only one which predicts the location and widths of

binary and recoil peaks, although not their height (figure 9). At constant θ_{ab} , for all but Cohen's distribution the (relative) magnitudes of the cross section for different angles are grossly wrong (figure 10). For the Wigner and the product distribution even the shape of the cross section is in disagreement with the experiment at $\theta_{ab} = 90^\circ$.

The cross sections at 17.6 eV show that even at this low total energy the fully differential cross section is sensitive to the initial phase space density. On the other hand, Wannier's arguments suggest that close to threshold the cross sections depend primarily on the final phase space configuration determined by the long-time behaviour of the ionization dynamics [60]. To describe it correctly, the accurate energy of the outgoing electrons is crucial. Hence, the initial distribution must have a minimal energy spread. At 4 eV above threshold, these two (contradicting) requirements are fulfilled best by Cohen's energy distribution.

5. Summary and outlook

We have derived and tested a quasiclassical ansatz for charged particle impact ionization. Starting from the time-dependent quantum mechanical formulation in the quantum Wigner picture, we can reproduce in the limit $\hbar = 0$ the standard CTMC method. However, our ansatz is more general. By keeping the backward-forward propagation scheme of the Møller formalism and by defining the cross section in terms of energy transfer, we can exploit the full classical limit ($\hbar = 0$) of the Wigner distribution for the initial state, which is neither stationary in the classical approximation nor confined to the energy shell, two properties which are necessary for the standard CTMC method. In fact, our formulation allows the use of arbitrary initial phase space distributions. We have calculated and compared fully differential classical ionization cross sections for four initial state distributions: the quantum Wigner function, the (standard) classical microcanonical distribution and two other distributions which interpolate to some extent between the Wigner and microcanonical distribution. From our results we conclude that at high impact energies the density in phase space is the crucial property for describing the ionization process. For lower energies the correlation between coordinate and momentum becomes increasingly important. Even at the low energy of 4 eV above threshold, the initial state has to be modelled correctly in coordinate and momentum space, although the long-time evolution of the slow ionized electrons gains more and more influence on the dynamics.

The classical calculations are not meant to be a high-quality substitute for quantum treatments; rather we wanted to formulate and test a consistent quasiclassical scattering theory, applicable to differential cross sections, and free from the limitation to one active target electron of previous approaches. Yet, most of the technical expertise from previous CTMC calculations can be used with only minor modifications in the description of the initial target state, the propagation scheme and the extraction of the cross sections.

With the present work we have demonstrated for one-electron targets, namely hydrogen, that the aforementioned goals can be achieved. However, the main advantage of being able to deal with unstable initial distributions will become apparent when calculating the double ionization of two-electron atoms. The classical autoionization of the bound electrons does not affect our quasiclassical approach. What should be improved in future work, particularly if one is interested in collisions with small excess energy, is the implementation of contributions off the energy shell. Since we have seen that fewer differential cross sections tend to be better approximated with the quasiclassical approach, we are optimistic that a quasiclassical triple differential cross section will be more accurate for double ionization than for single ionization. However, this remains to be proven in future work.

Acknowledgment

Most of this work was funded by the Deutsche Forschungsgemeinschaft through the SFB 276 at the University of Freiburg, Germany.

References

- [1] Ehrhardt H, Knoth G, Schlemmer P and Jung K 1985 *Phys. Lett. A* **110** 92
- [2] Ehrhardt H, Jung K, Knoth G and Schlemmer P 1986 *Z. Phys. D* **1** 3
- [3] Dal Cappello C, Tavad C, Lahmam-Bennani A and Dal Cappello M C 1984 *J. Phys. B: At. Mol. Phys.* **17** 4557
- [4] Brauner M, Briggs J S and Klar H 1989 *Z. Phys. D* **11** 257
- [5] Jones S, Madison D H and Srivastava H K 1992 *J. Phys. B: At. Mol. Opt. Phys.* **25** 1899
- [6] Berakdar J and Klar H 1993 *J. Phys. B: At. Mol. Opt. Phys.* **26** 3891
- [7] Wheelan C T, Walters H R J and Zhang X 1993 (*e, 2e*) and *Related Processes* ed C T Wheelan *et al* (Amsterdam: Kluwer)
- [8] Bray I and Stelbovics A T 1992 *Phys. Rev. A* **46** 6995
- [9] Rescigno T N, Baertschy M, Isaacs W A and McCurdy C W 1999 *Science* **286** 2474
- [10] Baertschy M, Rescigno T N, McCurdy C W, Colgan J and Pindzola M S 2001 *Phys. Rev. A* **63** 050701(R)
- [11] Baertschy M, Rescigno T N, Isaacs W A and McCurdy C W 2001 *Phys. Rev. A* **63** 022712
- [12] Isaacs W A, Baertschy M, McCurdy C W and Rescigno T N 2001 *Phys. Rev. A* **63** 030704(R)
- [13] Lahmam-Bennani A, Dupré C and Duguet A 1989 *Phys. Rev. Lett.* **63** 1582
- [14] Ullrich J, Moshhammer R, Dörner R, Jagutzki O, Mergel V, Schmidt-Böcking H and Spielberger L 1997 *J. Phys. B: At. Mol. Opt. Phys.* **30** 2917
- [15] Dörner R, Khemliche H, Prior M H, Cocke C L, Gary J A, Olson R E, Mergel V, Ullrich J and Schmidt-Böcking H 1996 *Phys. Rev. Lett.* **77** 4520
- [16] Dorn A, Moshhammer R, Schröter C D, Zouros T J M, Schmitt W, Kollmus H, Mann R and Ullrich J 1999 *Phys. Rev. Lett.* **82** 2496
- [17] Abrines R and Percival I C 1966 *Proc. Phys. Soc.* **88** 861
- [18] Eichenauer D, Grün N and Scheid W 1981 *J. Phys. B: At. Mol. Phys.* **14** 3929
- [19] Hardie D J W and Olson R E 1983 *J. Phys. B: At. Mol. Phys.* **16** 1983
- [20] Cohen J S 1985 *J. Phys. B: At. Mol. Phys.* **18** 1759
- [21] Raković M J, Schultz D R, Stancil P C and Janev R K 2001 *J. Phys. A: Math. Gen.* **34** 4753
- [22] McKenzie M L and Olson R E 1987 *Phys. Rev. A* **35** 2863
- [23] Olson R E, Ullrich J, Dörner R and Schmidt-Böcking H 1989 *Phys. Rev. A* **40** 2843
- [24] Schultz D R, Meng L and Olson R E 1992 *J. Phys. B: At. Mol. Opt. Phys.* **25** 4601
- [25] Kirschbaum C L and Wilets L 1980 *Phys. Rev. A* **21** 834
- [26] Zajfman D and Maor D 1986 *Phys. Rev. Lett.* **56** 320
- [27] Geyer T and Rost J M 2001 *J. Phys. B: At. Mol. Opt. Phys.* **34** L47
- [28] Wigner E 1932 *Phys. Rev.* **40** 749
- [29] John S and Remler R A 1987 *Ann. Phys., NY* **180** 152
- [30] Taylor J R 1972 *Scattering Theory* (New York: Wiley)
- [31] Heller E J 1976 *J. Chem. Phys.* **65** 1289
- [32] Keller S, Ast H and Dreizler R M 1993 *J. Phys. B: At. Mol. Opt. Phys.* **26** L737
- [33] Raff L M and Thompson D L 1985 *Theory of Chemical Reaction Dynamics* vol 3, ed M Baer (Boca Raton, FL: Chemical Rubber Company Press)
- [34] Dollard J D 1964 *J. Math. Phys.* **5** 729
- [35] Rost J M 1998 *Phys. Rep.* **297** 271
- [36] Carruthers P and Zachariasen F 1983 *Rev. Mod. Phys.* **55** 245
- [37] Moyal J E 1949 *Proc. Camb. Phil. Soc.* **45** 99
- [38] Mehta C L 1964 *J. Math. Phys.* **5** 677
- [39] Shewell J R 1959 *Am. J. Phys.* **27** 16
- [40] Cohen J S 1966 *J. Math. Phys.* **7** 781
- [41] Kustaanheimo P and Stiefel E 1965 *J. Reine Angew. Math.* **218** 204
- [42] Yoshida H 1990 *Phys. Lett. A* **150** 262
- [43] Shah M B, Elliot D S and Gilbody H B 1987 *J. Phys. B: At. Mol. Phys.* **20** 3501
- [44] Thomson J J Sir 1912 *Phil. Mag. Suppl.* **6** 23 449
- [45] Bethe H 1930 *Ann. Phys., NY* **5** 325

- [46] Shyn T W 1992 *Phys. Rev. A* **45** 2951
- [47] Roy A C 2001 *Nucl. Instrum. Methods B* **179** 163
- [48] Curran E P and Walters H R J 1987 *J. Phys. B: At. Mol. Phys.* **20** 337
- [49] McCarthy I E and Zhang X 1989 *J. Phys. B: At. Mol. Opt. Phys.* **22** 2189
- [50] Bray I 2000 *J. Phys. B: At. Mol. Opt. Phys.* **33** 581
- [51] Rost J M 1995 *J. Phys. B: At. Mol. Opt. Phys.* **28** 3003
- [52] Rost J M 1994 *Phys. Rev. Lett.* **72** 1998
- [53] Bray I 2000 *Aust. J. Phys.* **53** 355
- [54] Weigold E, Noble C J, Hood S T and Fuss I 1979 *J. Phys. B: At. Mol. Phys.* **12** 291
- [55] Lohmann B, McCarthy I E, Stelbovics A T and Weigold E 1984 *Phys. Rev. A* **30** 758
- [56] Lucey S P, Rasch J and Wheelan C T 1999 *Proc. R. Soc. A* **455** 349
- [57] Briggs J S 1989 *Comment. At. Mol. Phys.* **23** 155
- [58] Röder J, Rasch J, Jung K, Wheelan C T, Ehrhardt H, Allan R J and Walters H R J 1996 *Phys. Rev. A* **53** 225
- [59] Röder J, Jung K and Ehrhardt H 1993 *J. Physique IV* **3** 29
- [60] Wannier G H 1953 *Phys. Rev.* **90** 817